*American Mineralogist, Volume 76, pages 1306–1318, 1991*

# Mineralogy and geochemistry of Eocene intrusive rocks and their enclaves, El Paso area, Texas and New Mexico

Calvin G. Barnes, Susan E. Ensenat*
Department of Geosciences, Texas Tech University, Lubbock, Texas 79409, U.S.A.
James D. Hoover
Westinghouse Hanford Company, Richland, Washington 99352, U.S.A.

## Abstract

Trans-Pecos magmatism in the El Paso, Texas, area was characterized by numerous shallow trachyandesitic intrusions of Eocene age. Cognate enclaves in the intrusions consist of monzodiorite and porphyritic trachyandesite. The compositions of these enclaves indicate that they are cumulates formed near the margins of a crustal (possibly midcrustal) magma chamber. The mineral assemblages of the trachyandesitic and monzodioritic enclaves (tschermakitic amphibole + biotite + oxides + plagioclase ± titanite ± quartz) constrain preemplacement temperature to less than 850 °C and $f_{O_2}$ to 1 or 2 log units above NNO. $H_2O$ contents were probably in the range of 3.0 to 3.5 wt% and the confining pressure of the crustal chamber as much as 5.5 kbar (based on Al content of amphibole). Xenolithic enclaves include dioritic and anorthositic compositions. These are interpreted to be the wall rocks of the crustal chamber and are probably Precambrian in age. Incompatible element contents of the trachyandesitic magmas are interpreted to be the product of fractional crystallization of a subduction-related basaltic magma. Disequilibrium among phenocrysts in the trachyandesitic magmas and local enrichment of compatible elements can be explained by minor contamination by anorthositic and dioritic xenoliths.

## Introduction

Eocene hypabyssal intrusive rocks that crop out in the vicinity of El Paso, Texas, represent some of the oldest magmatic activity in the Trans-Pecos province (Hoover et al., 1988). These intrusions consist of porphyritic trachyandesite (classification of Le Bas et al., 1986) that is considerably more uniform in major and trace element compositions than other igneous suites in the province (e.g., Nelson et al., 1987; Henry and Price, 1986). Many of the intrusions contain enclaves (terminology of Didier, 1973) that range from trachyandesite nearly identical to the host rocks, through monzodiorite and diorite to anorthosite.

We present a description of the mineralogy of the intrusions and their enclaves. These data serve as indicators of the magmatic temperature and $f_{O_2}$, the degree of magma and enclave interaction, and in some cases, the depth of enclave crystallization. In addition, new major and trace element analyses of the samples provide constraints on the compositions of possible source regions.

## Summary of field relations

The intrusions crop out in a north-trending belt 10 km wide that extends from northern Chihuahua, Mexico, to north of El Paso, Texas (Fig. 1). They were emplaced in Lower Cretaceous sedimentary strata (Lovejoy, 1976; Hoover et al., 1988; Hoffer, 1970; Garcia, 1970; Chavez, 1986; Ensenat, 1989) during Eocene time (~47 Ma, three K-Ar dates on biotite; Hoover et al., 1988; Hoffer, 1970). In the southern part of the area, trachyandesite crops out as dikes and sills in the Sierra de Sapello and Sierra de Juarez ranges (Fig. 1; Hoover et al., 1988; Chavez, 1986). The central part of the area contains the largest intrusions; these include the thick (>100 m) sill-like Campus andesite (Hoffer, 1970) and smaller related bodies and the Sierra de Cristo Rey intrusion (Lovejoy, 1976; Ensenat, 1989). The Cristo Rey intrusion was interpreted to be a laccolith by Lovejoy (1976), but detailed study of enclave distributions within the pluton suggests a pluglike morphology (Ensenat, 1989; see below). A rhyolitic sill that crops out south and southwest of Cristo Rey (Fig. 2) dips radially away from Cristo Rey, indicating that it was domed by later intrusion of the Cristo Rey magma. The northern intrusions (herein referred to as the Three Sisters, Coronado, and Thunderbird sills; see Fig. 1) are also sill-like.

The magmas rose through a thick Precambrian section overlain by Paleozoic sedimentary rocks (principally carbonate). The upper part of the Precambrian section is exposed in adjacent fault blocks of the Franklin Mountains. It consists of siliciclastic and calc-silicate rocks and basaltic breccia overlain by weakly metamorphosed trachytic to rhyolitic lavas and ash-flow tuffs (Harbour, 1960,

* Present address: 1604 W. Dallas St., Artesia, New Mexico 88210, U.S.A.

0003–004X/91/0708–1306$02.00

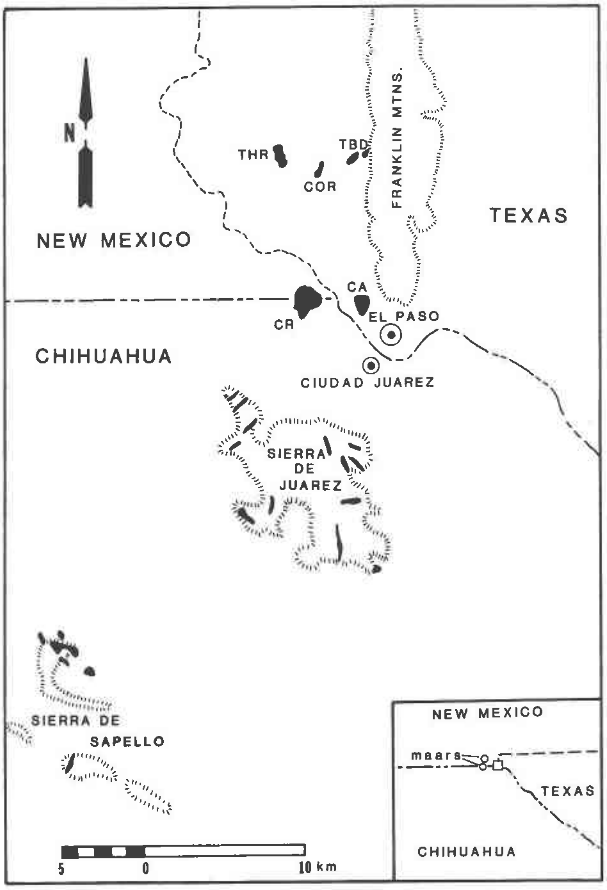


Fig. 1. Location map. Northern sills are Three Sisters (THR), Coronado (COR), and Thunderbird (TBD). Central intrusions are Sierra de Cristo Rey (CR), Campus andesite (CA), and University Plaza (not shown) just northeast of CA. Southern intrusions crop out in Sierra de Juarez and Sierra de Sapello. Inset shows location of Kilbourne Hole and Potrillo maar. After Hoover et al. (1988).

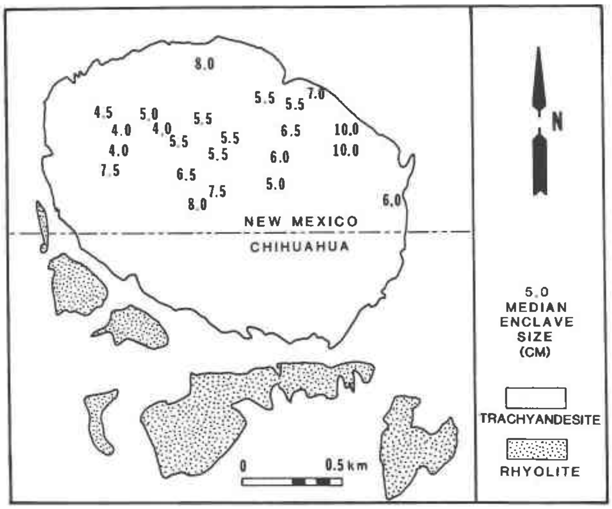


Fig. 2. Simplified geologic map of Sierra de Cristo Rey showing median diameter of monzodioritic enclaves and outcrop pattern of older rhyolitic sill. After Ensenat (1989) and Lovejoy (1976).

1972; Thomann, 1980). Alkali granites intruded all of these rocks at approximately 1.1 Ga (Shannon, 1989; Shannon and Barnes, 1989; Wasserburg et al., 1962; Copeland and Bowring, 1988).

## Enclaves

A variety of enclaves occur in the central and northern intrusions. They range in diameter from less than 0.5 cm to at least 1.2 m, with median diameters less than 10 cm. Rounded, spherical to oblate, medium-grained monzodiorite and quartz monzodiorite (Ensenat, 1989) is the most common enclave type, particularly in the Cristo Rey and Campus andesite intrusions (Fig. 2; Ensenat, 1989). This is the only enclave type with diameters larger than 22 cm. Some have thin (<5 mm) rims of biotite. Porphyritic trachyandesite forms a second but very sparse type of rounded, oblate enclave. These enclaves contain fewer phenocrysts than the host trachyandesite and were recognized only in the Cristo Rey intrusion.

The remaining enclave types are anorthositic and dioritic in composition. They are angular and are typically in sharp contact with trachyandesitic host rocks, but some occur as enclaves in monzodioritic enclaves.

Anorthositic enclaves range up to 22 cm in diameter and are the most abundant of the angular enclaves. They are weakly foliated to massive and range in composition from anorthosite to anorthositic gabbro and rarely gabbro. They are present in all of the northern and central intrusions and are particularly abundant in the Cristo Rey, Three Sisters, and Coronado bodies. They are absent in the southern intrusions. Clots of coarse- to very coarse-grained amphibole (1–5 cm in diameter) in the Cristo Rey and Three Sisters intrusions are interpreted to be from mafic zones or layers of the anorthositic enclaves.

Angular dioritic enclaves range from fine to coarse grained. In rare cases, host trachyandesite appears to be chilled against the diorite. Dioritic enclaves are particularly abundant in the Coronado and Three Sisters intrusions, where they range from 10 cm to less than 1 cm in diameter. Petrographically identical diorite occurs as thin dikes cutting anorthositic enclaves.

Ensenat (1989) interpreted the monzodiorite and rare trachyandesitic enclaves to be cognate (i.e., genetically related to the host trachyandesitic magma) on the basis of the lack of chilled host rock at contacts with these enclaves and the rounded nature of the enclaves. Anorthositic and dioritic enclaves (and amphibole clots) were interpreted to be xenoliths on the basis of their angular (broken) shapes and because the host trachyandesite is locally very fine grained against these enclaves.

Xenoliths of the host Cretaceous sedimentary rocks are rare. They consist of fine-grained hornfels and skarn, and they only occur near pluton margins.

TABLE 1. Summary of locations and petrographic features

| Mineral assemblage | Maximum dimension (mm) | Average abundance (vol%) | Notes |
|---|---|---|---|
| **Trachyandesitic host rocks** | | | |
| Phenocrysts | | | Fine-grained intergranular to subtrachytic groundmass. Ca amph ranges from equant to elongate (l/w = 14). Resorbed cores in northern intrusions. Accessory Fe-Ti oxides, apatite, zircon. |
| Calcic amphibole | 5 | 12 | |
| Biotite | 3 | 2 | |
| Plagioclase | 3 | 28 | |
| Quartz | 1 | <1 | |
| Groundmass | | 56 | |
| **Porphyritic trachyandesitic enclaves** | | | |
| Phenocrysts | | | In Cristo Rey intrusion. Rounded, oblate shape. Fine-grained intergranular groundmass. Ca amph typically elongate (l/w = 9). Accessory Fe-Ti oxides, apatite, zircon. Accessory apatite and zircon typically elongate (l/w = 20); apatite commonly hollow; rare acicular apatite and zircon. |
| Calcic amphibole | 3 | 15 | |
| Biotite | 3 | 2 | |
| Plagioclase | 2 | 17 | |
| Groundmass | | 65 | |
| **Monzodioritic enclaves** | | | |
| Calcic amphibole | 5 | | In central and northern intrusions. Rounded, oblate, lack cuspate margins. Medium-grained hypidiomorphic granular ave. grain size 1.5 mm. Ca amph ranges from equant to elongate (l/w = 14). Accessory Fe-Ti oxides, apatite, zircon, titanite. Contains 0.5 mm stubby apatite and acicular apatite to 1.2 mm. |
| Biotite | 5 | | |
| Plagioclase | 3 | | |
| Sanidine | 1 | | |
| Quartz | 1 | | |
| **Anorthositic xenoliths** | | | |
| Calcic amphibole | 10 | | In Three Sisters, Coronado, Cristo Rey, and Campus Andesite intrusions. Sharp, angular contacts with host. Highly variable modal proportions. Accessory titanite. Commonly deformed. |
| Clinopyroxene | 5 | | |
| Plagioclase | >100 | | |
| Ilmenite | 2 | | |
| **Dioritic xenoliths** | | | |
| Calcic amphibole | 2 | | In Three Sisters, Coronado, Cristo Rey, and Campus Andesite intrusions; as rare dikes in anorthositic xenoliths. Sharp, angular contacts. Variable modal proportions and grain size (fine to medium). Foliated to massive. Accessory Fe-Ti oxides, acicular apatite. |
| Biotite | 0.5 | | |
| Plagioclase | 2 | | |

### Enclave distribution in the Cristo Rey intrusion

Lovejoy (1976) interpreted the Cristo Rey intrusion to be a laccolith. However, faint flow foliation and flow banding in the intrusion are steeply dipping or vertical. This orientation is not compatible with laccolithic style of intrusion (Corry, 1988). The distribution and size of enclaves were measured in an attempt to understand better the shape and style of intrusion of the Cristo Rey body. Only monzodioritic and anorthositic enclaves were abundant enough (40–400 enclaves per site) to yield useful population data. For these equidimensional to slightly oblate enclave types, the median length of the long axis decreases from the margin to the central part of the pluton. Enclaves with the smallest diameters occur northwest of the center of the pluton (Fig. 2). Inward decrease of enclave size is consistent with intrusion as a diapir (e.g., Castro, 1987) with in situ ballooning toward the southeast. Diapiric emplacement followed by ballooning is also consistent with steeply dipping flow foliation and banding.

## PETROGRAPHY

Detailed petrographic descriptions are presented in Hoover et al. (1988), Ensenat (1989), Garcia (1970), and Hoffer (1970). The main petrographic features are summarized in Table 1.

The trachyandesitic host rocks contain phenocrysts of tschermakitic amphibole, biotite, plagioclase, and quartz with microphenocrysts of apatite, ilmenite, altered magnetite, and rare zircon. The groundmass consists of intergranular to subtrachytic arrangements of plagioclase, alkali feldspar, quartz, biotite, oxide minerals, and zircon. In the Three Sisters sill, amphibole and clinopyroxene are rare groundmass phases. Porphyritic trachyandesite enclaves are similar to the host rocks (Table 1).

The rhyolitic sill at Cristo Rey consists of very fine-grained quartz and altered feldspars. No mafic minerals are present in this rock because of the effects of weathering and hydrothermal(?) alteration.

Monzodioritic enclaves are medium-grained hypidiomorphic granular (average grain size ~1 mm) and consist of blocky plagioclase and sanidine, equant to elongate subhedral tschermakitic amphibole, subhedral biotite, and anhedral quartz, and rare clinopyroxene (Table 1). Plagioclase-rich monzodioritic samples contain fine-grained interstitial material similar to the groundmass of the host trachyandesite. K-rich members of this group contain resorbed plagioclase replaced by sanidine, indicative of low-$T$ reaction of plagioclase with residual felsic liquid (e.g., Carmichael et al., 1974; Nekvasil, 1990). Interstitial orthoclase and granophyre are locally present in these samples.

Anorthositic xenoliths consist of varying proportions of sutured plagioclase (~$An_{48}$, with bent or broken twin lamellae) and interstitial tschermakitic amphibole, clinopyroxene, and ilmenite. Trails of clinopyroxene mark healed fractures in plagioclase grains in some samples. These textures are typical of high-temperature protoclastic deformation and recrystallization. The effects of immersion of anorthositic xenoliths in host trachyandesite are locally apparent as intergranular growth of biotite and amphibole, as titanite rims on ilmenite, and at enclave margins, as rims of plagioclase typical of the host (~$An_{35}$) around plagioclase typical of the anorthosite (~$An_{48}$).

**TABLE 2.** Summary of plagioclase compositions

| Sample | Enclave type | Enclave plag comp. (An%) Range* | Enclave plag comp. (An%) Zoning | Host plag comp. (An%) Range* | Host plag comp. (An%) Zoning |
|---|---|---|---|---|---|
| | | **Cerro de Cristo Rey** | | | |
| CRSTR4 | | | | 33–28 | N |
| CR79B | | | | 41–23 | N |
| CR2B | diorite | 35–24 | ? | | |
| CR81EN | diorite | 42–38 | N | | |
| CR5E | porph. tr. | 23 (ave) | | | |
| CR7F | anorthosite | 41–36 | N | | |
| | | **Three Sisters** | | | |
| THR3 | anorthosite | 44 (ave) | | | |
| THR5 | anorthosite | 41 (ave) | | 35–28 | N |
| THR7 | anorthosite | 48 (ave) | | | |
| THR17 | anorthosite | 47 (ave) | | 48–31 | R |
| C5 | anorthosite | 53 (ave) | | 36–28 | N |
| | | **Coronado** | | | |
| CO18 | anorthosite | 43–19 | N | 31–28 | N |
| CO21 | | | | 37–26 | N |
| CO22 | anorthosite | 48 (ave) large xtal<br>39–49, small xtal | | | |
| | | **University Plaza** | | | |
| UNIPA | | | | 29–18 | N |
| | | **Sierra de Juarez** | | | |
| SDJ1 | | | | 36–26 | R |

*Note:* Zoning classified as normal (N), reversed (R).

**TABLE 3.** Clinopyroxene analyses

| | CO20 cpx1 | CO20 cpx3 | THR17 cpx1 | THR17 cpx2 |
|---|---|---|---|---|
| | | **Oxide wt%** | | |
| $SiO_2$ | 52.2 | 52.9 | 51.3 | 51.7 |
| $TiO_2$ | 0.29 | 0.18 | 0.59 | 0.48 |
| $Al_2O_3$ | 1.32 | 0.85 | 2.13 | 2.09 |
| FeO | 7.53 | 9.09 | 10.6 | 10.3 |
| MnO | 0.43 | 0.64 | 0.39 | 0.32 |
| MgO | 13.8 | 13.0 | 12.8 | 12.8 |
| CaO | 23.1 | 23.0 | 21.6 | 21.7 |
| $Na_2O$ | 0.54 | 0.59 | 0.48 | 0.47 |
| Total | 99.28 | 100.16 | 99.83 | 99.89 |
| | | **Cations per six O atoms** | | |
| Si | 1.960 | 1.981 | 1.934 | 1.945 |
| Ti | 0.008 | 0.005 | 0.017 | 0.014 |
| Al | 0.058 | 0.038 | 0.095 | 0.093 |
| Fe | 0.237 | 0.285 | 0.334 | 0.325 |
| Mn | 0.014 | 0.020 | 0.012 | 0.010 |
| Mg | 0.775 | 0.724 | 0.717 | 0.718 |
| Ca | 0.931 | 0.921 | 0.874 | 0.874 |
| Na | 0.039 | 0.043 | 0.035 | 0.034 |
| Sum | 4.022 | 4.017 | 4.019 | 4.013 |

## ANALYTICAL METHODS

Mineral compositions were determined with a JEOL JXA-733 electron microprobe at Southern Methodist University, using natural and synthetic standards and a modified Bence-Albee data reduction scheme. Whole-rock major element and Rb contents were determined by atomic absorption spectroscopy at Texas Tech. The remaining trace elements were analyzed by INAA at the University of Texas at El Paso (see Hoover et al., 1988, for analytical procedure).

## MINERALOGY

### Plagioclase

Phenocrysts in the trachyandesite typically display oscillatory-normal zoning in the range $An_{41}$–$An_{18}$ (Table 2); however, most crystals range from $An_{36}$ to $An_{23}$. Reverse zoning is common only in plagioclase from the Three Sisters sill ($An_{31}$–$An_{48}$). Plagioclase from monzodioritic enclaves and dioritic xenoliths are $An_{35}$–$An_{24}$; however, individual crystals lack appreciable zoning.

Plagioclase in anorthositic xenoliths is unzoned or normally zoned. Compositions range from $An_{53}$ to $An_{19}$ but are typically $>An_{40}$. Anorthite contents less than $An_{40}$ are generally from crystals at or near the contact between the anorthositic enclave and the host.

### Clinopyroxene

Clinopyroxene in anorthositic xenoliths from Three Sisters and Coronado are salitic to diopsidic. The pyroxenes are Al and Na poor, with less than 0.1 and 0.05 cations per formula unit, respectively (Table 3).

### Amphibole

Most amphiboles are tschermakite or tschermakitic hornblende (Table 4; Fig. 3A). Structural formulas (calculated according to the algorithm of Spear and Kimball, 1984) indicate that the $Fe^{3+}$ content of these amphiboles is low. An excellent correlation exists among $^{[4]}Al$ and the sum of A-site cations, $^{[6]}Al$, $Fe^{3+}$, and (2 × Ti) (not shown). This indicates that cation substitution is dominated by the Tschermak component. No correlation is present between $^{[4]}Al$ and the acmite component (sum of A-site cations minus $^{[M4]}Na$).

Two broad groups of amphibole compositions can be distinguished (Fig. 3). The first group has Mg/(Mg + Fe) greater than 0.6 and Na/(Na + K) greater than 0.78, and it consists of amphibole phenocrysts from the trachyandesitic host rocks and amphiboles from monzodioritic enclaves. In detail, phenocrysts from the Three Sisters sill are distinctly bimodal and plot in discrete groups, whereas samples from the Coronado sill plot in a broad zone (Fig. 3A). Amphiboles from Cristo Rey and most amphiboles from the Three Sisters trachyandesite display good correlation between Mg/(Mg + Fe) and Si per formula unit (Fig. 3A).

The second amphibole group has Mg/(Mg + Fe) less than 0.6 and Na/(Na + K) less than 0.78 (owing to larger K contents). This group consists of amphibole from anorthositic xenoliths and encompasses the compositions of amphiboles from some dioritic xenoliths, a porphyritic trachyandesite enclave, and some of the amphibole phenocrysts in the Three Sisters and Coronodo sills.

Rims of actinolitic hornblende are present in some monzodioritic and dioritic enclaves (Fig. 3A). These rims are interpreted to represent subsolidus or near solidus growth during slow cooling.

**TABLE 4.** Representative amphibole compositions

| Sample | Phenocrysts from trachyandesite | | | | | | | | Porph. | |
|---|---|---|---|---|---|---|---|---|---|---|
| | CR79b core | CRSTR4 rim | CRSTR4 mantle | CO21 mantle | THR17 rim | THR17 rim | C5 core | C5 core | CR5e core | CR5e rim |
| | | | | Oxide wt% | | | | | | |
| $SiO_2$ | 42.3 | 42.9 | 42.4 | 42.6 | 43.1 | 40.3 | 44.9 | 42.9 | 42.2 | 40.1 |
| $Al_2O_3$ | 12.0 | 11.8 | 12.4 | 12.0 | 13.0 | 15.0 | 10.5 | 12.1 | 11.9 | 13.8 |
| FeO | 9.36 | 8.78 | 10.8 | 11.1 | 8.94 | 13.9 | 8.82 | 10.3 | 12.8 | 13.5 |
| MgO | 15.3 | 16.0 | 13.8 | 13.1 | 14.9 | 10.8 | 15.7 | 14.3 | 12.8 | 11.4 |
| $TiO_2$ | 1.87 | 2.57 | 2.37 | 2.85 | 2.80 | 2.41 | 2.51 | 2.66 | 1.43 | 2.06 |
| MnO | 0.09 | 0.12 | 0.10 | 0.23 | 0.10 | 0.21 | 0.14 | 0.21 | 0.42 | 0.23 |
| BaO | 0.07 | 0.06 | 0.10 | 0.05 | 0.06 | 0.05 | 0.04 | 0.07 | 0.07 | 0.07 |
| CaO | 14.0 | 11.8 | 11.6 | 11.4 | 11.4 | 10.8 | 10.9 | 11.5 | 11.1 | 11.5 |
| $Na_2O$ | 2.61 | 2.48 | 2.50 | 2.66 | 2.69 | 2.66 | 2.47 | 2.65 | 2.42 | 2.57 |
| $K_2O$ | 0.74 | 0.75 | 0.86 | 0.76 | 0.75 | 1.02 | 0.83 | 0.98 | 1.16 | 0.79 |
| Cl | 0.02 | 0.00 | 0.05 | 0.04 | 0.02 | 0.10 | 0.04 | 0.04 | 0.06 | 0.07 |
| F | 0.13 | 0.31 | 0.06 | 0.34 | 0.53 | 0.26 | 0.20 | 0.09 | 0.39 | 0.09 |
| Total | 98.43 | 97.56 | 97.16 | 97.03 | 98.26 | 97.55 | 97.1 | 97.84 | 96.75 | 96.19 |
| | | | | Cations per 23 O atoms | | | | | | |
| Si | 6.172 | 6.257 | 6.267 | 6.298 | 6.222 | 6.014 | 6.532 | 6.286 | 6.331 | 6.083 |
| Al | 2.066 | 2.026 | 2.160 | 2.086 | 2.209 | 2.648 | 1.804 | 2.092 | 2.101 | 2.468 |
| Fe | 1.143 | 1.070 | 1.333 | 1.375 | 1.080 | 1.741 | 1.073 | 1.266 | 1.607 | 1.707 |
| Mg | 3.332 | 3.470 | 3.046 | 2.892 | 3.208 | 2.402 | 3.405 | 3.118 | 2.860 | 2.577 |
| Ti | 0.205 | 0.282 | 0.263 | 0.317 | 0.304 | 0.271 | 0.275 | 0.293 | 0.161 | 0.235 |
| Mn | 0.011 | 0.015 | 0.013 | 0.029 | 0.012 | 0.027 | 0.017 | 0.026 | 0.053 | 0.030 |
| Ba | 0.004 | 0.003 | 0.006 | 0.003 | 0.003 | 0.003 | 0.002 | 0.004 | 0.004 | 0.004 |
| Ca | 2.186 | 1.834 | 1.842 | 1.803 | 1.762 | 1.730 | 1.706 | 1.798 | 1.777 | 1.859 |
| Na | 0.739 | 0.701 | 0.716 | 0.763 | 0.753 | 0.770 | 0.697 | 0.752 | 0.704 | 0.755 |
| K | 0.138 | 0.139 | 0.162 | 0.144 | 0.138 | 0.194 | 0.154 | 0.183 | 0.222 | 0.153 |
| Cl | 0.005 | 0.000 | 0.013 | 0.010 | 0.005 | 0.025 | 0.010 | 0.010 | 0.015 | 0.018 |
| F | 0.060 | 0.143 | 0.028 | 0.159 | 0.242 | 0.123 | 0.092 | 0.042 | 0.185 | 0.043 |
| Total | 16.061 | 15.940 | 15.849 | 15.880 | 15.939 | 15.948 | 15.767 | 15.869 | 16.020 | 15.932 |
| Mg/(Mg + Fe) | 74.5 | 76.4 | 69.6 | 67.8 | 74.8 | 58.0 | 76.0 | 71.1 | 64.0 | 60.2 |

*Note:* Porph. is porphyritic trachyandesite enclave, gb. anorth. is gabbroic anorthosite enclave.

## Biotite

Most biotite crystals were nonstoichiometric due to loss of K. The stoichiometric analyses (Table 5) indicate that biotite Mg/(Mg + Fe) ranges from 0.56 to 0.64 and averages 0.60. Ba contents are relatively large (up to 1.5 wt% BaO), and F and Cl contents are negligible.

**TABLE 5.** Biotite compositions

| | CO18 | CO21 | CO22 | SDJ1 | CR2B |
|---|---|---|---|---|---|
| | | | Oxide wt% | | |
| $SiO_2$ | 36.0 | 36.5 | 35.7 | 36.3 | 36.3 |
| $TiO_2$ | 4.35 | 4.24 | 4.00 | 3.54 | 3.33 |
| $Al_2O_3$ | 14.6 | 14.8 | 15.6 | 15.8 | 15.9 |
| FeO | 16.2 | 14.5 | 15.6 | 15.4 | 13.6 |
| MnO | 0.23 | 0.18 | 0.22 | 0.18 | 0.20 |
| MgO | 13.9 | 14.6 | 13.3 | 13.5 | 15.0 |
| CaO | 0.01 | 0.02 | 0.00 | 0.00 | 0.14 |
| BaO | 0.91 | 0.97 | 0.73 | 1.05 | 1.02 |
| $Na_2O$ | 0.50 | 0.79 | 0.65 | 0.89 | 0.51 |
| $K_2O$ | 8.39 | 8.31 | 8.29 | 8.23 | 8.16 |
| Cl | 0.09 | 0.08 | 0.09 | 0.06 | 0.07 |
| F | 0.22 | 0.13 | 0.00 | 0.12 | 0.32 |
| Total | 95.32 | 95.14 | 94.15 | 94.97 | 94.51 |
| | | | Cations per 22 O atoms | | |
| Si | 5.465 | 5.502 | 5.446 | 5.485 | 5.472 |
| Ti | 0.495 | 0.477 | 0.456 | 0.399 | 0.376 |
| Al | 2.603 | 2.625 | 2.801 | 2.818 | 2.818 |
| Fe | 2.060 | 1.816 | 1.982 | 1.939 | 1.716 |
| Mn | 0.026 | 0.022 | 0.026 | 0.022 | 0.022 |
| Mg | 3.134 | 3.279 | 3.021 | 3.031 | 3.357 |
| Ca | 0.000 | 0.000 | 0.000 | 0.000 | 0.022 |
| Ba | 0.053 | 0.053 | 0.040 | 0.062 | 0.057 |
| Na | 0.147 | 0.229 | 0.188 | 0.262 | 0.146 |
| K | 1.623 | 1.595 | 1.611 | 8.230 | 1.566 |
| Cl | 0.022 | 0.018 | 0.018 | 0.060 | 0.013 |
| F | 0.102 | 0.062 | 0.000 | 0.120 | 0.150 |
| Total | 15.729 | 15.677 | 15.589 | 15.669 | 15.716 |

## GEOCHEMISTRY

The trachyandesitic intrusions are, in general, typical of high-K calc-alkaline magmas (Table 6; Gill and Whelan, 1989), although a few samples are potassic enough to plot in the extension of the low-K shoshonite field (Fig. 4). With the exception of the Cristo Rey rhyolite, the intrusive suite and cognate enclaves display a relatively small range of $SiO_2$ contents (Fig. 5). They are $Al_2O_3$ rich (Fig. 5C), as is typical of calc-alkaline suites. In plots of $SiO_2$ vs. $TiO_2$, MgO, and $Na_2O$, the compositions of most dioritic and anorthositic xenoliths do not plot on the trend defined by the trachyandesite and cognate enclaves (Fig. 5).

Trace element compositions (Table 7; Figs. 6–8; also see Hoover et al., 1988) are characterized by the relatively high concentrations of Sr, Ba, Rb, and LREE and low concentrations of Y, Nb, and Ta that are typical of high-K calc-alkaline suites (e.g., Gill, 1981). The Ba content of anorthositic and dioritic xenoliths is much lower than that of the trachyandesitic host and the cognate monzodioritic enclaves (Fig. 6). The two groups also plot on distinct trends. In the Sr-Ba plot, two dioritic samples plot with the trachyandesitic rocks; these diorites (samples CR2B and CRMA) are the samples that contain amphibole similar to amphibole phenocrysts in the trachyandesite.

**TABLE 4**—*Continued*

| Monzodiorite | | Diorite | | | | Gb. anorth. | | Anorthosite | | | |
|---|---|---|---|---|---|---|---|---|---|---|---|
| CR69 mantle | CR69 rim | CR49 core | CR49 mantle | CR2b rim | CR2b mantle | CR81 core | CR81 mantle | CR7f mantle | CR7f rim | CR7f core | THR17 core |
| Oxide wt% | | | | | | | | | | | |
| 42.6 | 41.5 | 39.8 | 40.9 | 48.5 | 43.8 | 39.6 | 39.5 | 44.1 | 43.3 | 42.5 | 41.6 |
| 11.5 | 13.1 | 14.8 | 14.1 | 5.59 | 12.5 | 14.8 | 14.3 | 9.40 | 10.1 | 10.6 | 11.9 |
| 8.51 | 12.2 | 12.7 | 10.7 | 11.2 | 9.80 | 12.1 | 17.6 | 16.0 | 17.2 | 16.0 | 14.8 |
| 16.1 | 13.2 | 11.7 | 13.0 | 15.3 | 14.7 | 11.5 | 8.50 | 11.1 | 10.2 | 10.8 | 11.1 |
| 2.16 | 2.52 | 2.41 | 2.48 | 1.71 | 1.72 | 2.43 | 1.63 | 1.11 | 1.43 | 1.59 | 2.77 |
| 0.11 | 0.17 | 0.18 | 0.11 | 0.40 | 0.15 | 0.12 | 0.33 | 0.54 | 0.43 | 0.45 | 0.16 |
| 0.07 | 0.04 | 0.07 | 0.11 | 0.03 | 0.07 | 0.07 | 0.07 | 0.00 | 0.00 | 0.07 | 0.08 |
| 10.6 | 11.1 | 10.7 | 11.1 | 11.5 | 11.9 | 11.1 | 11.2 | 11.3 | 10.2 | 10.3 | 11.6 |
| 2.61 | 2.64 | 2.67 | 2.71 | 1.59 | 2.53 | 2.63 | 2.16 | 1.91 | 2.08 | 2.07 | 2.23 |
| 0.86 | 0.78 | 1.11 | 1.09 | 0.52 | 0.79 | 0.76 | 1.27 | 0.87 | 0.96 | 1.08 | 1.45 |
| 0.02 | 0.02 | 0.05 | 0.03 | 0.12 | 0.02 | 0.04 | 0.09 | 0.07 | 0.08 | 0.09 | 0.29 |
| 0.00 | 0.26 | 0.25 | 0.30 | 0.36 | 0.00 | 0.29 | 0.18 | 0.03 | 0.34 | 0.16 | 0.00 |
| 96.15 | 97.43 | 96.46 | 96.64 | 96.77 | 97.95 | 95.42 | 96.82 | 96.34 | 96.21 | 95.74 | 97.94 |
| Cations per 23 O atoms | | | | | | | | | | | |
| 6.414 | 6.145 | 5.988 | 6.082 | 7.114 | 6.361 | 5.999 | 6.070 | 6.705 | 6.608 | 6.512 | 6.239 |
| 1.987 | 2.280 | 2.632 | 2.473 | 0.967 | 2.144 | 2.638 | 2.593 | 1.683 | 1.820 | 1.920 | 2.113 |
| 1.046 | 1.516 | 1.598 | 1.335 | 1.370 | 1.191 | 1.528 | 2.255 | 2.026 | 2.193 | 2.055 | 1.861 |
| 3.531 | 2.914 | 2.621 | 2.879 | 3.349 | 3.183 | 2.604 | 1.946 | 2.501 | 2.320 | 2.457 | 2.479 |
| 0.239 | 0.281 | 0.273 | 0.277 | 0.189 | 0.188 | 0.277 | 0.188 | 0.127 | 0.164 | 0.183 | 0.313 |
| 0.014 | 0.021 | 0.023 | 0.014 | 0.050 | 0.018 | 0.015 | 0.043 | 0.069 | 0.056 | 0.058 | 0.020 |
| 0.004 | 0.002 | 0.004 | 0.006 | 0.002 | 0.004 | 0.004 | 0.004 | 0.000 | 0.000 | 0.004 | 0.005 |
| 1.665 | 1.758 | 1.723 | 1.769 | 1.801 | 1.858 | 1.805 | 1.845 | 1.833 | 1.663 | 1.691 | 1.861 |
| 0.744 | 0.759 | 0.779 | 0.781 | 0.452 | 0.713 | 0.773 | 0.643 | 0.563 | 0.616 | 0.615 | 0.649 |
| 0.161 | 0.148 | 0.213 | 0.207 | 0.097 | 0.147 | 0.147 | 0.249 | 0.169 | 0.187 | 0.211 | 0.278 |
| 0.005 | 0.005 | 0.013 | 0.008 | 0.030 | 0.005 | 0.010 | 0.023 | 0.018 | 0.021 | 0.023 | 0.074 |
| 0.000 | 0.122 | 0.119 | 0.141 | 0.167 | 0.000 | 0.139 | 0.087 | 0.014 | 0.164 | 0.078 | 0.000 |
| 15.809 | 15.951 | 15.985 | 15.973 | 15.588 | 15.812 | 15.939 | 15.947 | 15.708 | 15.812 | 15.808 | 15.892 |
| 77.1 | 65.8 | 62.1 | 68.3 | 71.0 | 72.8 | 63.0 | 46.3 | 55.2 | 51.4 | 54.5 | 57.1 |

**TABLE 6.** Representative major element compositions

| Sample | Oxide wt%, normalized to 100 | | | | | | | | | | |
|---|---|---|---|---|---|---|---|---|---|---|---|
| | $SiO_2$ | $TiO_2$ | $Al_2O_3$ | $Fe_2O_3$ | FeO | MnO | MgO | CaO | $Na_2O$ | $K_2O$ | $P_2O_5$ | LOI |
| Trachyandesite | | | | | | | | | | | | |
| CR6F | 61.9 | 0.72 | 17.2 | 2.54 | 2.22 | 0.09 | 2.29 | 4.28 | 5.29 | 2.95 | 0.48 | 1.83 |
| CR7F | 63.7 | 0.61 | 17.2 | 1.62 | 2.23 | 0.07 | 1.62 | 3.48 | 5.88 | 3.08 | 0.48 | 0.90 |
| CRSTR7 | 63.5 | 0.57 | 18.4 | 2.29 | 1.32 | 0.07 | 1.43 | 3.45 | 5.75 | 2.85 | 0.45 | 1.37 |
| CR74A | 61.7 | 0.70 | 18.0 | 3.34 | 1.15 | 0.08 | 1.80 | 3.94 | 5.89 | 2.98 | 0.44 | 1.15 |
| CR79A | 62.2 | 0.63 | 17.8 | 3.00 | 1.12 | 0.09 | 2.13 | 4.08 | 5.81 | 2.66 | 0.41 | 1.12 |
| CR79B | 62.3 | 0.66 | 17.7 | 3.01 | 1.14 | 0.09 | 1.75 | 4.13 | 5.72 | 2.99 | 0.46 | 1.26 |
| COR2 | 59.3 | 0.90 | 16.6 | 6.03 | n.d. | 0.09 | 4.17 | 4.54 | 5.20 | 2.75 | 0.38 | n.d. |
| COR86 | 59.3 | 0.89 | 16.6 | 5.77 | n.d. | 0.09 | 3.95 | 4.45 | 5.55 | 3.03 | 0.40 | n.d. |
| THR86 | 62.7 | 0.66 | 17.9 | 4.02 | n.d. | 0.06 | 2.01 | 3.91 | 5.22 | 3.30 | 0.29 | n.d. |
| UNI86 | 63.5 | 0.50 | 18.4 | 3.60 | n.d. | 0.06 | 1.38 | 3.57 | 6.16 | 2.49 | 0.30 | n.d. |
| CA | 64.8 | 0.48 | 17.8 | 3.38 | n.d. | 0.06 | 1.30 | 3.32 | 6.04 | 2.54 | 0.28 | n.d. |
| SDJ | 64.2 | 0.53 | 17.3 | 4.07 | n.d. | 0.06 | 1.81 | 4.40 | 3.94 | 3.38 | 0.28 | n.d. |
| SDJ1 | 63.4 | 0.52 | 18.7 | 3.57 | n.d. | 0.07 | 1.36 | 4.30 | 6.15 | 1.52 | 0.36 | n.d. |
| Rhyolite | | | | | | | | | | | | |
| FE1 | 74.3 | 0.04 | 15.2 | 0.13 | n.d. | 0.02 | 0.10 | 0.67 | 5.23 | 4.36 | 0.03 | n.d. |
| FE2 | 74.3 | 0.05 | 13.6 | 1.36 | n.d. | 0.04 | 0.55 | 0.63 | 4.93 | 4.30 | 0.14 | 1.89 |
| Porphyritic trachyandesite | | | | | | | | | | | | |
| CR5E | 60.0 | 0.83 | 18.5 | 2.05 | 3.16 | 0.16 | 1.79 | 4.47 | 5.34 | 3.04 | 0.71 | 2.22 |
| Monzodiorite | | | | | | | | | | | | |
| CR40A | 61.1 | 0.81 | 17.0 | 3.47 | 1.88 | 0.11 | 2.16 | 4.81 | 5.31 | 2.88 | 0.53 | 2.03 |
| 69ENY | 59.8 | 0.90 | 16.6 | 5.70 | n.d. | 0.11 | 3.72 | 6.04 | 4.98 | 1.75 | 0.41 | 2.44 |
| CR69EN | 60.4 | 0.92 | 17.4 | 3.34 | 2.30 | 0.10 | 2.74 | 4.45 | 5.37 | 2.41 | 0.56 | 2.35 |
| CRFLEN | 61.8 | 0.89 | 17.4 | 2.88 | 2.22 | 0.10 | 1.83 | 3.67 | 5.53 | 3.07 | 0.58 | 1.86 |
| Anorthosite | | | | | | | | | | | | |
| CR15B | 54.4 | 0.81 | 18.3 | 5.08 | 2.53 | 0.18 | 3.72 | 7.83 | 5.54 | 0.86 | 0.48 | 1.61 |
| CR82A | 57.1 | 0.67 | 20.3 | 2.91 | 2.56 | 0.13 | 2.12 | 6.47 | 6.17 | 1.03 | 0.48 | 0.45 |
| THR189 | 61.9 | 0.59 | 19.3 | 3.26 | n.d. | 0.07 | 0.50 | 2.39 | 5.28 | 6.52 | 0.24 | n.d. |
| THR101 | 54.6 | 0.96 | 23.4 | 3.94 | n.d. | 0.06 | 1.47 | 9.23 | 5.72 | 0.49 | 0.13 | n.d. |
| C5 | 51.2 | 1.87 | 23.4 | 5.34 | n.d. | 0.09 | 2.29 | 10.30 | 4.67 | 0.70 | 0.05 | n.d. |
| Diorite | | | | | | | | | | | | |
| CR2B | 48.0 | 1.39 | 17.4 | 4.28 | 6.07 | 0.21 | 8.97 | 8.07 | 3.36 | 1.82 | 0.48 | n.d. |
| CRMA | 44.0 | 1.28 | 17.6 | 14.15 | n.d. | 0.24 | 7.27 | 11.53 | 2.80 | 0.68 | 0.41 | n.d. |
| CO25 | 52.8 | 1.09 | 15.2 | 7.08 | n.d. | 0.20 | 5.82 | 10.70 | 5.12 | 1.58 | 0.39 | n.d. |

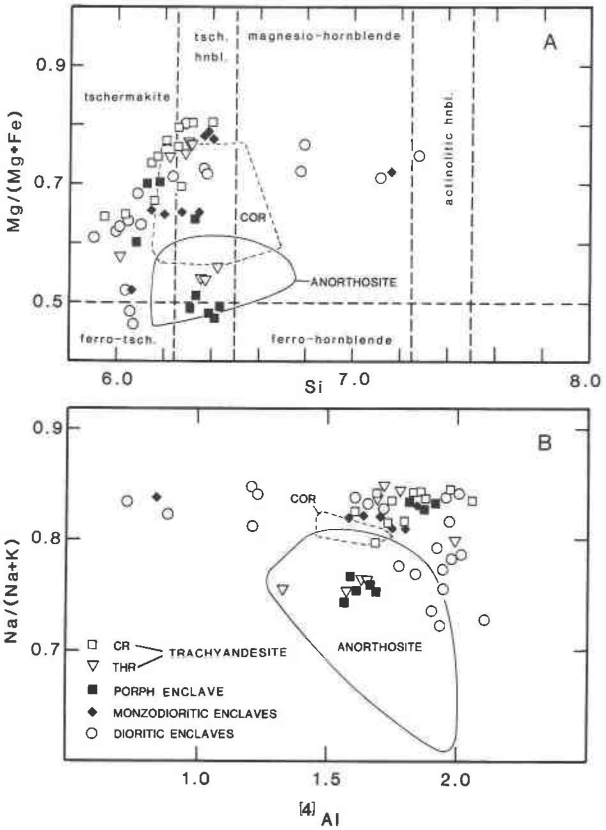


Fig. 3. Amphibole compositions. All cation proportions per 23 O atoms. Fields shown for amphiboles from Coronado sill (COR) and anorthositic enclaves. (**A**) Variation of Mg/(Mg + Fe) with Si; (**B**) variation of Na/(Na + K) with Al in tetrahedral sites.

The trachyandesitic intrusions can be subdivided on the basis of trace element compositions (Hoover et al., 1988). The central intrusions contain relatively larger abundances of Sr at a given Ba concentration (Fig. 6A)

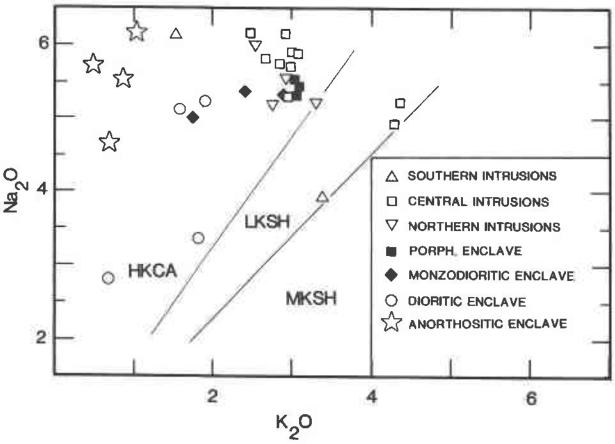


Fig. 4. Alkali contents of trachyandesite and enclaves. Fields shown are from Gill and Whelan (1989): high-K calc-alkaline (HKCA), low-K shoshonitic (LKSH), and medium-K shoshonitic (MKSH).

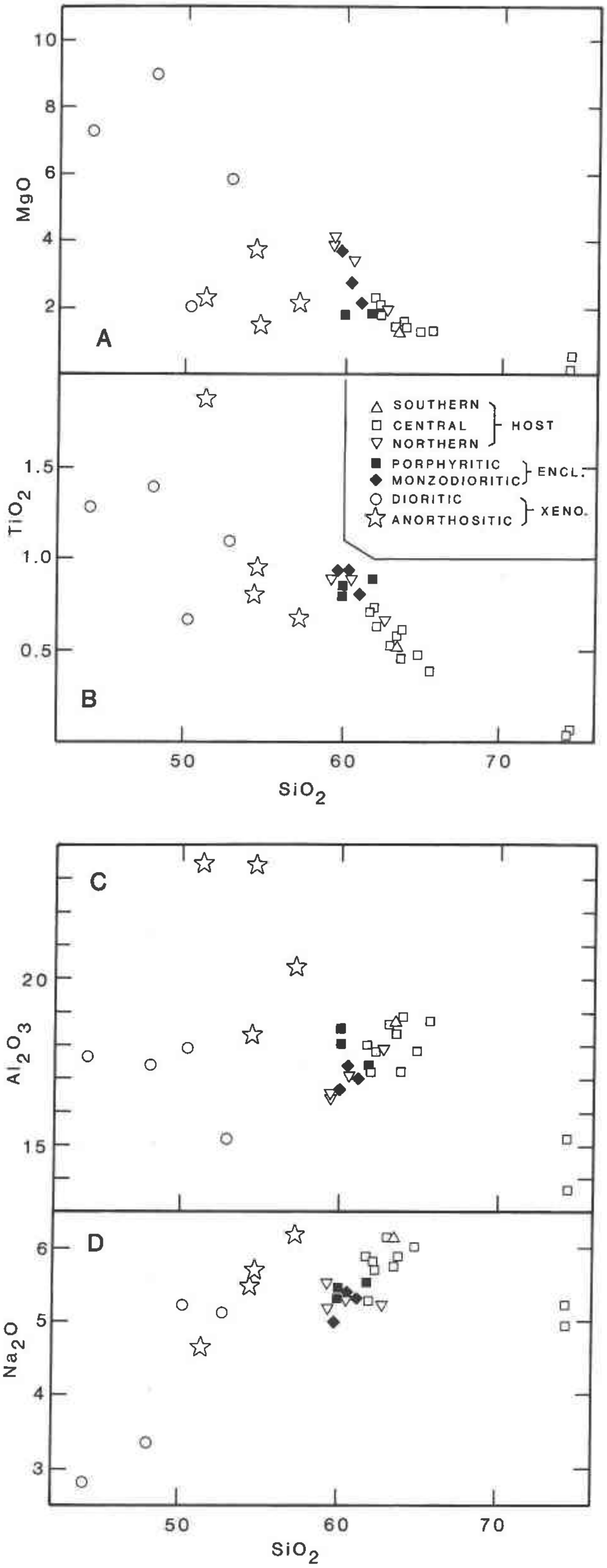


Fig. 5. Major element variation as a function of $SiO_2$ content. (**A**) MgO; (**B**) $TiO_2$; (**C**) $Al_2O_3$; (**D**) $Na_2O$. Porphyritic and monzodioritic enclaves are cognate; dioritic and anorthositic enclaves are xenolithic.

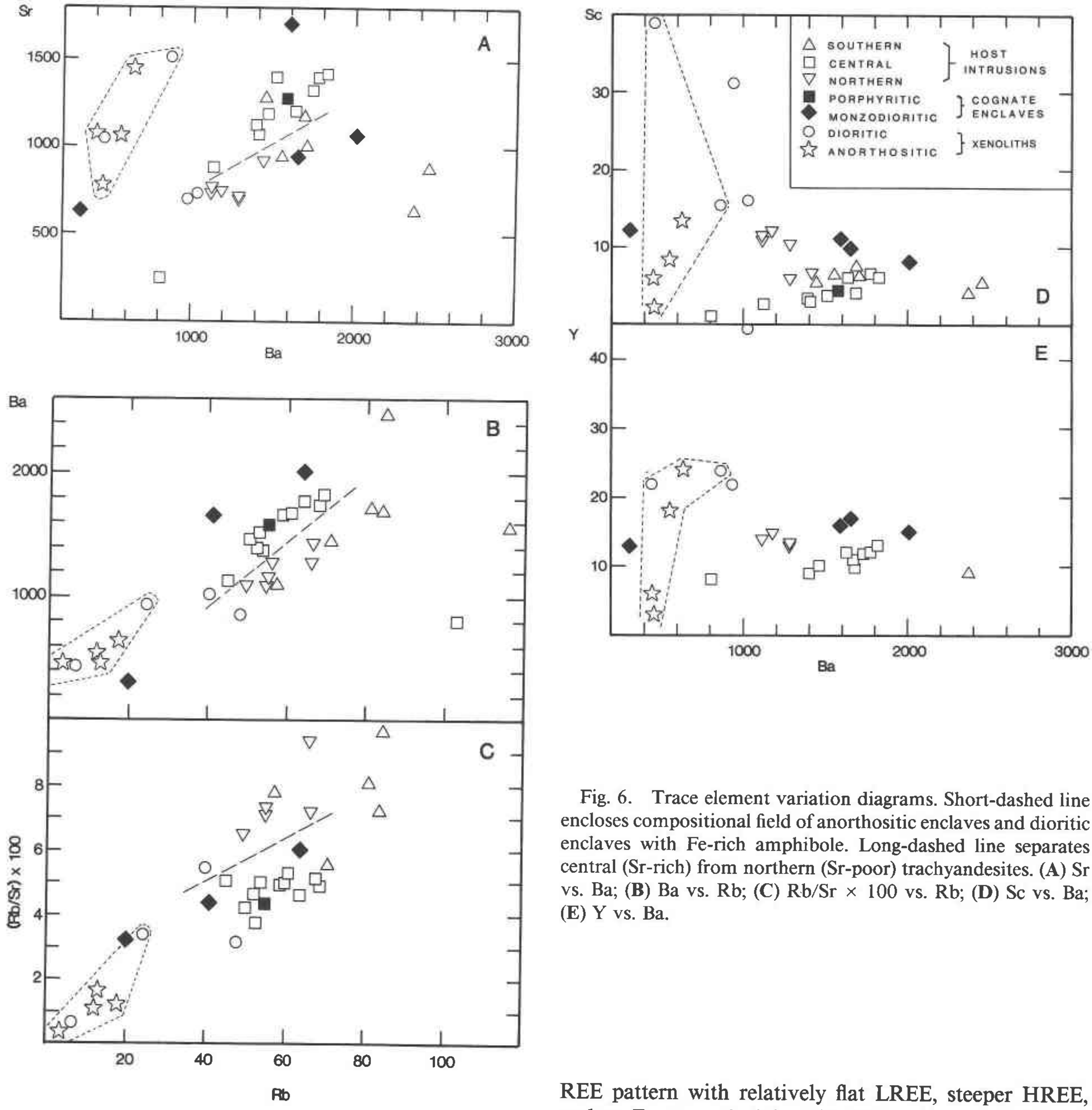


Fig. 6. Trace element variation diagrams. Short-dashed line encloses compositional field of anorthositic enclaves and dioritic enclaves with Fe-rich amphibole. Long-dashed line separates central (Sr-rich) from northern (Sr-poor) trachyandesites. (**A**) Sr vs. Ba; (**B**) Ba vs. Rb; (**C**) Rb/Sr × 100 vs. Rb; (**D**) Sc vs. Ba; (**E**) Y vs. Ba.

and generally have $Ce_N/Yb_N$ between 14 and 22. The northern intrusions contain less Sr but higher concentrations of Sc, Cr, V, and Y(?) at a given Ba concentration and higher Rb/Sr ratios than the central intrusions (Fig. 6). $Ce_N/Yb_N$ in the northern group ranges from 10.5 to 15. Samples from the southern part of the area plot with both groups.

The moderately steep REE patterns of the trachyandesitic host rocks show little or no inflection and no Eu anomaly (Fig. 7A). The difference in $Ce_N/Yb_N$ between northern and central sills cited above is largely due to variations in Yb content. In contrast, the rhyolitic intrusion at Cristo Rey contains lower REE abundances than the trachyandesitic intrusions. It also displays an unusual REE pattern with relatively flat LREE, steeper HREE, and no Eu anomaly (Fig. 7A). This pattern probably reflects loss of LREE during alteration and weathering.

The REE pattern of the porphyritic trachyandesite enclave from Cristo Rey is identical to that of the host rocks (Fig. 7B). Monzodioritic enclave REE patterns have slopes similar to the host trachyandesites but contain somewhat lower REE abundances.

Anorthosite xenoliths contain lower abundances of REE, have $Ce_N/Yb_N$ less than 12, and display pronounced positive Eu anomalies (Fig. 8C).

Dioritic enclaves have $Ce_N/Yb_N$ less than 12 and generally less than 6. The two enclaves that are chemically and mineralogically similar to the trachyandesite (CR2B and CRMA) contain lower LREE abundances than do the other dioritic samples (Fig. 7C). Although plagioclase

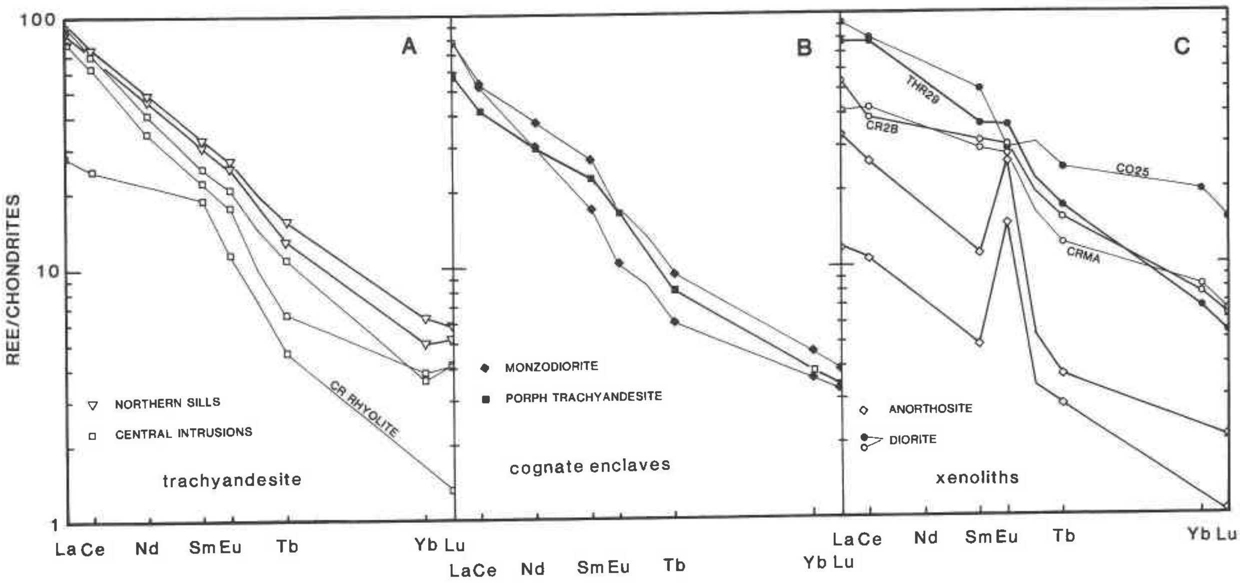


Fig. 7. Chondrite-normalized (Haskin et al., 1968) rare earth element plots. (**A**) Trachyandesitic and rhyolitic intrusions; (**B**) monzodioritic enclaves and porphyritic trachyandesitic enclave; (**C**) dioritic and anorthositic enclaves.

phenocrysts are sparse or absent in the dioritic enclaves, three display slight positive Eu anomalies.

### Incompatible element patterns

The trachyandesitic rocks plot in a narrow band on "spider diagrams" (Fig. 8A; normallization factors of Thompson et al., 1984). Porphyritic trachyandesitic and monzodioritic enclaves have similar patterns (Figs. 8B and 8D).

Dioritic and anorthositic xenoliths have distinctly different patterns from the trachyandesite (Figs. 8C and 8D), in keeping with their xenolithic character.

## Discussion

### Intensive variables

Qualitative estimates of the $T$ and $f_{O_2}$ of the trachyandesitic magmas can be made on the basis of comparison

**Table 7.** Representative trace element concentrations

| | La | Ce | Nd | Sm | Eu | Tb | Yb | Lu | Sc | Cr | Co |
|---|---|---|---|---|---|---|---|---|---|---|---|
| | | | | | **Trachyandesite** | | | | | | |
| CR6f | 21.6 | 40.7 | 23.3 | 4.2 | 1.03 | 0.40 | 0.80 | 0.12 | 6.1 | 40 | 10 |
| CR74A | | | | | | | | | 6.7 | 32 | |
| CR79A | | | | | | | | | 6.2 | 32 | |
| CR79B | | | | | | | | | 6.3 | 40 | |
| CRIST3 | 26.0 | 54.9 | 20.6 | 4.0 | 1.21 | 0.31 | 0.77 | 0.14 | 3.8 | 17 | 72 |
| CRIST3 | 30.4 | 61.7 | 24.4 | 4.5 | 1.42 | 0.51 | 0.72 | 0.14 | 4.2 | 12 | 29 |
| | | | | | **Rhyolite** | | | | | | |
| FE1 | 9.2 | 21.5 | | 3.4 | 0.78 | 0.22 | | 0.04 | 1.1 | 1 | 0 |
| | | | | | **Porphyritic trachyandesite** | | | | | | |
| CR5E | 18.9 | 36.7 | 17.8 | 4.1 | 1.13 | 0.38 | 0.77 | 0.12 | 4.5 | 4 | 8 |
| | | | | | **Monzodiorite** | | | | | | |
| CR10A | 26.1 | 45.0 | 17.5 | 3.1 | 0.71 | 0.28 | 0.72 | 0.11 | 1.2 | 3 | 2 |
| CR13A | 25.9 | 46.2 | 22.3 | 4.8 | 1.19 | 0.44 | 0.91 | 0.13 | 7.0 | 39 | 12 |
| CR40A | | | | | | | | | 8.1 | 2 | |
| CR69ENY | | | | | | | | | 11.0 | 48 | |
| CR69ENZ | | | | | | | | | 9.8 | 13 | |
| CR72AEN | | | | | | | | | 12.1 | 122 | |
| | | | | | **Diorite** | | | | | | |
| CO25 | 30.2 | 70.0 | | 8.9 | 2.00 | 1.13 | 3.90 | 0.51 | 16.0 | 175 | 21 |
| CR2B | 17.6 | 33.6 | | 5.6 | 2.05 | 0.72 | 1.52 | 0.21 | 31.3 | 316 | 34 |
| CRMA | 13.5 | 36.9 | | 5.2 | 1.88 | 0.57 | 1.63 | 0.22 | 39.0 | 9 | 42 |
| THR29 | 25.3 | 67.0 | | 6.5 | 2.45 | 0.80 | 1.34 | 0.18 | 15.5 | 149 | 27 |
| | | | | | **Anorthositic gabbro** | | | | | | |
| CR82A | | | | | | | | | 8.4 | 0 | |
| | | | | | **Anorthosite** | | | | | | |
| THR10 | 10.8 | 22.5 | | 2.0 | 1.77 | 0.17 | | 0.07 | 6.0 | 2 | 9 |
| C5 | 3.9 | 9.3 | | 0.9 | 1.00 | 0.13 | | 0.03 | 2.4 | 10 | 19 |

*Note:* Blank entry indicates element not determined.

with experimental studies. The presence of early-formed amphibole phenocrysts is suggestive of $H_2O$ contents of 3.0 to 3.5 wt% (Eggler, 1972). Quartz and biotite phenocrysts in magmas with comparable $H_2O$ contents are stable at $T$ less than 800 °C and probably at less than 750 °C (Piwinskii, 1968, 1973; Whitney, 1975; Naney, 1983).

The presence of coexisting Fe-Ti oxide phenocrysts in the trachyandesite is characteristic of moderate to high $f_{O_2}$ (e.g., Wones, 1981; Czamanske et al., 1981), as is the high Mg/(Mg + Fe) of amphibole and biotite and the positive correlation between Mg/(Mg + Fe) and Si in amphibole from the Cristo Rey intrusion (e.g., Czamanske et al., 1981). In support of this inference, it can be noted that the assemblage calcic amphibole + magnetite + titanite + quartz + ilmenite is present in several monzodioritic (cognate) enclaves. It corresponds to $f_{O_2}$ conditions between 1 and 2 log units higher than the NNO buffer (Noyes et al., 1983). Similar conditions of crystallization are reasonable in view of the similarity of mineral and elemental compositions. Although coexisting Fe-Ti oxide phenocrysts are present, subsolidus exsolution and alteration have rendered these phases useless for determination of $T$ and $f_{O_2}$.

K-rich monzodioritic enclaves contain the assemblage calcic amphibole + biotite + plagioclase + alkali feldspar ± quartz + magnetite ± titanite ± ilmenite. If equilibrium was attained with near-minimum interstitial melt, then the Al content of calcic amphiboles is pressure dependent (Hammarstrom and Zen, 1986; Hollister et al., 1987). The average Al content (cations per formula unit) of the rims of magmatic amphibole from appropriate monzodioritic enclaves is 2.12 ± 0.15 ($1\sigma$). This value corresponds to a pressure of 5.5 kbar (Johnson and Rutherford calibration, 1989) and an estimated depth of crystallization of the monzodioritic enclaves of 16 km, with minimum uncertainty of ±4 km. By contrast, the probable depth of emplacement (estimated on the basis of stratigraphic reconstruction) was less than 2 km.

### Mass balance calculations

Fractional crystallization relationships among rock types in the Cristo Rey intrusion were tested for major element compositions with least-squares mass-balance calculations (Bryan et al., 1969). Parent-daughter relationships that were tested include diorite (sample CR2B) to trachyandesite, monzodiorite to trachyandesite, trachyandesite to rhyolite, and low-Si trachyandesite to high-Si trachyandesite (Table 8). None of the attempts to produce trachyandesite from dioritic enclave magma was successful. Evolved trachyandesite can be produced from magma of monzodioritic composition by removal of plagioclase + amphibole ± magnetite ± ilmenite and from less evolved trachyandesite by removal of amphibole + minor plagioclase ± apatite. The rhyolite can be derived from evolved trachyandesite by removal of plagioclase, amphibole, biotite, magnetite, and apatite. This calculation requires removal of approximately 51% crystals (by weight). Unfortunately, when acceptable (i.e., sum of squares of residuals < 1.0) mass balance solutions are examined in detail, they either fail to fit important elements adequately (especially $TiO_2$, $P_2O_5$, and $Na_2O$), or the daughter product is not typical of the bulk of the trachyandesites. In addition, fractional crystallization cannot explain the positive correlation of Sc and Ba and

TABLE 7—*Continued*

| Ni | Rb | Sr | Zr | Nb | Ba | Cs | Hf | U | Th | Ta | Y |
|---|---|---|---|---|---|---|---|---|---|---|---|
| | | | | | **Trachyandesite** | | | | | | |
| 30 | 68 | 1328 | 158 | 3 | 1736 | 1.62 | 3.28 | 1.71 | 4.49 | 0.51 | 12 |
| 16 | 64 | 1403 | 149 | 3 | 1777 | | | | | | 12 |
| 25 | 60 | 1201 | 138 | 3 | 1633 | | | | | | 12 |
| 33 | 61 | 1163 | 143 | 3 | 1678 | | | | | | 11 |
| 12 | 52 | 1126 | 142 | 6 | 1390 | 2.84 | 3.87 | 1.38 | 3.97 | 1.46 | |
| 13 | 59 | 1189 | 143 | 6 | 1684 | 2.04 | 4.41 | 1.62 | 4.04 | 0.86 | 10 |
| | | | | | **Rhyolite** | | | | | | |
| 0 | 103 | 242 | 62 | 3 | 808 | 1.26 | 2.44 | 2.04 | 1.25 | 1.39 | 8 |
| | | | | | **Porphyritic trachyandesite** | | | | | | |
| 12 | 55 | 1270 | 132 | 6 | 1580 | 1.06 | 2.70 | 1.34 | 2.86 | 0.26 | |
| | | | | | **Monzodiorite** | | | | | | |
| 10 | 31 | 1065 | 114 | 5.5 | 521 | 8.62 | 3.08 | 1.09 | 4.60 | 0.48 | |
| 28 | 35 | 1190 | 161 | 5.4 | 522 | 6.76 | 3.15 | 1.46 | 4.21 | 0.47 | |
| 0 | 64 | 1062 | 143 | 5 | 2013 | | | | | | 15 |
| 32 | 33 | 1707 | 157 | 5 | 1595 | | | | | | 16 |
| 6 | 41 | 941 | 152 | 5 | 1657 | | | | | | 17 |
| 55 | 20 | 627 | 111 | 5 | 312 | | | | | | 13 |
| | | | | | **Diorite** | | | | | | |
| 82 | 40 | 730 | 63 | 7 | 1036 | 1.58 | 1.70 | 0.64 | 1.78 | 0.37 | 45 |
| 33 | 24 | 700 | 84 | 15 | 940 | 1.70 | 3.00 | 0.69 | 1.47 | | 22 |
| 13 | 7 | 1037 | 65 | 18 | 449 | 2.10 | 1.33 | 0.27 | 0.56 | | 22 |
| 22 | 48 | 1510 | 49 | 6 | 864 | 1.83 | 1.39 | 0.31 | 0.80 | | 24 |
| | | | | | **Anorthositic gabbro** | | | | | | |
| 0 | 12 | 1056 | 112 | 5 | 554 | | | | | | 18 |
| | | | | | **Anorthosite** | | | | | | |
| 0 | 4 | 1013 | 56 | 1 | 461 | 0.55 | 1.03 | 0.10 | 0.36 | 0.12 | 6 |
| 58 | 13 | 772 | 26 | 3 | 468 | 1.73 | 0.32 | 0.18 | 0.23 | | 3 |

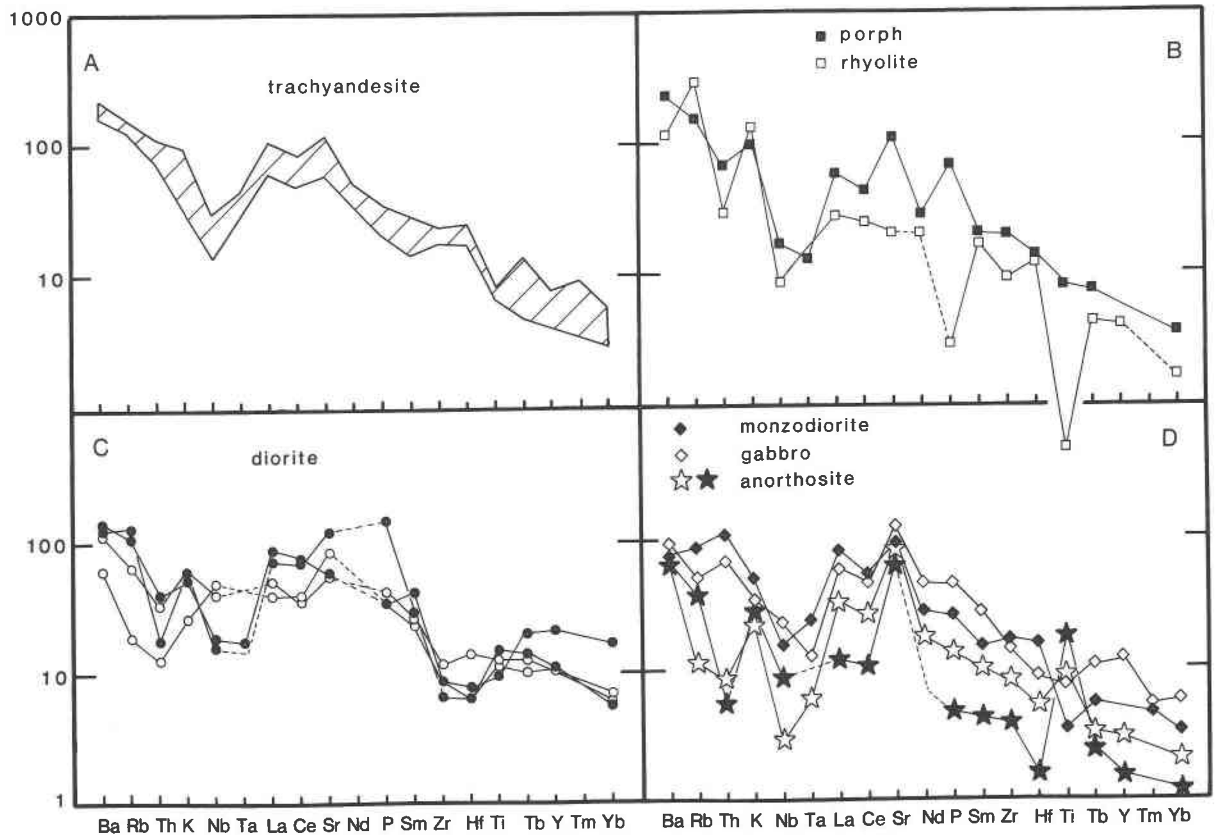


Fig. 8. Incompatible element variation diagrams; normalization factors from Thompson et al. (1984). (**A**) Typical field for trachyandesitic intrusions. (**B**) Compositions of porphyritic trachyandesite enclave (porph) and rhyolitic intrusion south of Cristo Rey. (**C**) Dioritic compositions; filled symbols represent dioritic enclaves with Fe-rich amphibole; open symbols represent dioritic enclaves with Mg-rich amphibole similar to host trachyandesite. (**D**) Compositions of cognate monzodioritic enclaves and xenolithic anorthosite and anorthositic gabbro (gabbro).

of Y and Ba among samples from the Cristo Rey intrusion (Figs. 6D and 6E).

The scatter observed in many variation diagrams suggests that problems in obtaining acceptable solutions to mass balance calculations may be because of variable degrees of crystal accumulation (see Hoover et al., 1988). The scatter is particularly apparent in plots of $Al_2O_3$, Sr, and compatible trace elements (Figs. 5 and 6). If crystal sorting and accumulation occurred during flow and emplacement of the trachyandesitic magma, then the effects of both fractional crystallization and crystal accumulation would be present in the suite. Part of the scatter observed in the northern sills, particularly the higher concentrations of Sc, Cr, Ni, and MgO, can also be explained as contamination by dioritic and anorthositic xenoliths. Such contamination would be the result of fragmentation and resorption of the xenoliths and would explain the increase in compatible element concentrations in samples

**Table 8.** Results of mass-balance calculations

| | | Phases removed | | | | | | | | |
|---|---|---|---|---|---|---|---|---|---|---|
| Parent | Daughter | Amph. | Biotite | Plag. | AP | MT | ILM | $F$ | $R^2$ | Notes |
| CR6F trach. | CR7F trach. | 7.5 | — | 4.3 ($AN_{35}$) | 0.3 | — | — | 87.9 | 0.33 | poor fit for Na |
| CR6F trach. | CR7F trach. | 7.2 | — | 3.7 ($An_{58}$) | 0.1 | — | — | 89.0 | 0.20 | poor fit for Na, plag too calcic |
| 69ENZ monzo. | CR7F trach. | 12.8 | — | 7.9 ($An_{44}$) | — | — | 0.4 | 78.9 | 0.37 | poor fit for P, with or without apatite |
| CR7F trach. | FE2 rhyo. | 4.1 | 6.8 | 37.2 ($An_{36}$) | 1.1 | 1.5 | — | 49.4 | 0.83 | poor fit for Na |
| CR7F trach. | FE2 rhyo. | 6.2 | 6.2 | 38.0 ($An_{29}$) | 1.3 | 1.2 | — | 47.1 | 0.40 | poor fit for Na and Mn |

*Note:* Abbreviations are trachyandesite (trach.), monzodiorite (monzo.), rhyolite (rhyo.).

of the host trachyandesite. The calcic plagioclase and the resorbed, Fe-rich amphibole in the northern intrusions are probably xenocrysts broken from dioritic and anorthositic xenoliths. Finally, the low abundance of incompatible elements (especially LREE) in the rhyolite suggests equilibrium with LREE-rich accessory minerals, either in the source or during fractional crystallization.

### Origin of the enclaves

The presence of deformed crustal xenoliths within some cognate monzodioritic enclaves indicates that they began to crystallize from the trachyandesitic magma along the margins of a magma chamber. If $P$ estimates are correct, this chamber was in the middle crust. In any case, slow cooling and crystallization of the monzodioritic rocks resulted in hypidiomorphic granular texture and in prismatic habits of accessory minerals. Parts of this monzodioritic rind were engulfed in and disrupted by the trachyandesitic magma as it rose to the site of final emplacement in the shallow crust.

The anorthositic xenoliths (and most dioritic xenoliths) are distinct from the host trachyandesite in terms of plagioclase and amphibole compositions and in Ba, Sr, REE, and HFSE concentrations. The fact that these xenoliths occur not only in the host trachyandesite but also in cognate monzodioritic enclaves suggests that the wall rocks of the midcrustal trachyandesite magma reservoir(s) were predominantly anorthositic and dioritic.

## Conclusions

The trachyandesitic intrusions in the El Paso area were emplaced at high levels in the crust after possible residence in the middle crust. The trachyandesitic magma was emplaced at temperatures of 850 °C or lower, contained approximately 3.0 wt% $H_2O$, and had $f_{O_2}$ 1 to 2 log units higher than NNO.

The wall rocks of the magma chamber consisted, at least in part, of anorthosite and related diorite and anorthositic gabbro. The presence of weakly deformed anorthosite in the crust beneath the El Paso area is consistent with widespread occurrence of Proterozoic anorthosite in the southwestern United States (e.g., Emslie, 1978; Anderson, 1983; McLemore and McKee, 1988; Padovani and Carter, 1977). It seems likely that anorthositic xenoliths in the trachyandesites represent an as-yet unrecognized segment of Precambrian crust in the area.

As the trachyandesite broke out of its crustal chamber, it incorporated part of its mostly crystalline rind to form monzodioritic enclaves and also engulfed anorthositic and dioritic wall rocks. Disruption of these rocks and contamination of the host trachyandesite resulted in bimodal compositions among amphibole populations and in elevated abundances of compatible elements in the northern sills.

The elemental abundances (i.e., enriched LILE, negative slope, and relatively depleted HFSE) of the trachyandesitic intrusions display patterns that are typical of continental arc magmas (Fig. 8; Gill, 1981; Thompson et al., 1984). As such, these rocks represent early manifestations of Tertiary arc activity in the Trans-Pecos of western Texas. Further constraints on magma sources will require detailed isotopic investigations.

## Acknowledgments

We are grateful to T. Frost, R. Wiebe, C. Bacon, T. Prestvik, and R. Cullers for helpful reviews, to B. May and W.M. Shannon for assistance in the field, and to M.A. Barnes for help in the laboratory. S.E.E.'s field studies were funded by the New Mexico Bureau of Mines and Mineral Resources, the Penrose bequest from the Geological Society of America, and Texas Tech University. Analyses were funded by NSF grants EAR-840319 and EAR-8720141 (C.G.B.).

## References cited

Anderson, J.L. (1983) Proterozoic anorogenic granite plutonism of North America. Geological Society of America Memoir, 161, 133–154.

Bryan, W.B., Finger, L.W., and Chayes, F. (1969) Estimating proportions in petrographic mixing equations by least squares approximation. Science, 163, 926–927.

Carmichael, I.S.E., Turner, F.J., and Verhoogen, J. (1974) Igneous Petrology, 739 p. McGraw-Hill, New York.

Castro, A. (1987) On granitoid emplacement and related structures. A review. Geologische Rundschau, 76, 101–124.

Chavez, R. (1986) Stratigraphy and structural geology of the Sierra de Sapello, northern Chihuahua, Mexico, 167 p. M.S. thesis, University of Texas at El Paso, El Paso, Texas.

Copeland, P., and Bowring, S.A. (1988) U-Pb zircon and $^{40}Ar/^{39}Ar$ ages from Proterozoic rocks, West Texas. Geological Society of America Abstracts with Programs, 20, 95–96.

Corry, C.E. (1988) Laccoliths: mechanics of emplacement and growth. Geological Society of America Special Paper, 220, 110 p.

Czamanske, G.K., Ishihara, S., and Atkin, S.A. (1981) Chemistry of rock-forming minerals of the Cretaceous-Paleocene batholith in southwestern Japan and implications for magma genesis. Journal of Geophysical Research, 86, 10431–10469.

Didier, J. (1973) Granites and their enclaves: The bearing of enclaves on the origin of granites, 393 p. Elsevier, New York.

Eggler, D.H. (1972) Water-saturated and undersaturated melting relations in a Paricutin andesite and an estimate of water content in the natural magma. Contributions to Mineralogy and Petrology, 34, 261–271.

Emslie, R.F. (1978) Anorthosite massifs, rapakivi granites, and Late Proterozoic rifting of North America. Precambrian Research, 7, 61–98.

Ensenat, S.E. (1989) Geology and geochemistry of Sierra de Cristo Rey and its inclusions, Dona Ana County, New Mexico, 109 p. M.S. thesis, Texas Tech University, Lubbock, Texas.

Garcia, R.A. (1970) Geology and petrography of andesitic intrusions in and near El Paso, Texas, 139 p. M.S. thesis, University of Texas at El Paso, El Paso, Texas.

Gill, J.B. (1981) Orogenic andesites and plate tectonics, 390 p. Springer-Verlag, New York.

Gill, J.B., and Whelan, P. (1989) Early rifting of an oceanic island arc (Fiji) produced shoshonitic to tholeiitic basalts. Journal of Geophysical Research, 94, 4561–4578.

Hammarstrom, J.M., and Zen, E-an (1986) Aluminum in hornblende: An empirical igneous geobarometer. American Mineralogist, 71, 1297–1313.

Harbour, R.L. (1960) Precambrian rocks at North Franklin Mountain, Texas. Bulletin of the American Association of Petroleum Geologists, 44, 1785–1792.

——— (1972) Geology of the northern Franklin Mountains, Texas and New Mexico. U.S. Geological Survey Bulletin, 1298, 129 p.

Haskin, L.A., Haskin, M.A., Frey, F.A., and Wildeman, T.R. (1968) Relative and absolute terrestrial abundances of the rare earths. In L.H. Ahrens, Ed., Origin and distribution of the elements, p. 889–912. Pergamon, Oxford, United Kingdom.

Henry, C.D., and Price, J.G. (1986) Early Basin and Range development in Trans-Pecos Texas and adjacent Chihuahua: Magmatism and orientation, timing and style of extension. Journal of Geophysical Research, 91, 6213–6224.

Hoffer, J.M. (1970) Petrology and mineralogy of the Campus Andesite Pluton, El Paso, Texas. Geological Society of America Bulletin, 81, 2129–2136.

Hollister, L.S., Grissom, G.C., Peters, E.K., Stowell, H.H., Sisson, V.B. (1987) Confirmation of the empirical correlation of Al in hornblende with pressure of solidification of calc-alkaline plutons. American Mineralogist, 72, 231–239.

Hoover, J.D., Ensenat, S.B., Barnes, C.G., and Dyer, R. (1988) Early Trans-Pecos magmatism: Petrology and geochemistry of Eocene intrusive rocks in the El Paso area. In G.H. Mack, T.F. Lawton, and S.G. Lucas, Eds., Cretaceous and Laramide tectonic evolution of southwestern New Mexico, p. 109–118. New Mexico Geological Society, Socorro, New Mexico.

Johnson, M.C., and Rutherford, M.J. (1989) Experimental calibration of the aluminum-in-hornblende geobarometer with application to Long Valley caldera (California) volcanic rocks. Geology, 17, 837–841.

Le Bas, M.J., Le Maitre, R.W., Strecheisen, A., and Zanettin, B. (1986) A chemical classification of volcanic rocks based on the total alkali-silica diagram. Journal of Petrology, 27, 745–750.

Lovejoy, E.M.P. (1976) Geology of Cerro de Cristo Rey uplift, Chihuahua and New Mexico, New Mexico Bureau of Mines and Mineral Resources, Memoir 31, 84 p.

McLemore, V.T., and McKee, C. (1988) A preliminary geochemical study of the Redrock anorthosite and granite, Burro Mountains, southwestern New Mexico. In G.H. Mack, T.F. Lawton, and S.G. Lucas, Eds., Cretaceous and Laramide tectonic evolution of southwestern New Mexico, p. 83–88. New Mexico Geological Society, Socorro, New Mexico.

Naney, M.T. (1983) Phase equilibria of rock-forming silicates in granitic systems. American Journal of Science, 283, 993–1033.

Nekvasil, H. (1990) Reaction relations in the granite system: Implications for trachytic and syenitic magmas. American Mineralogist, 75, 560–571.

Nelson, D.O., Nelson, K.L., Reeves, K.D., and Mattison, G.D. (1987) Geochemistry of Tertiary alkaline rocks of the eastern Trans-Pecos magmatic province, Texas. Contributions to Mineralogy and Petrology, 97, 72–92.

Noyes, H.J., Wones, D.R., and Frey, F.A. (1983) A tale of two plutons: Petrographic and mineralogic constraints on the petrogenesis of the Red Lake and Eagle Peak plutons, central Sierra Nevada, California. Journal of Geology, 91, 353–379.

Padovani, E.R., and Carter, J.L. (1977) Aspects of the deep crustal evolution beneath south central New Mexico. In J.G. Heacock, Ed., The Earth's crust, it's nature and physical properties, p. 19–55. American Geophysical Union, Washington, DC.

Piwinskii, A.J. (1968) Experimental studies of igneous rock series, central Sierra Nevada batholith, California. Journal of Geology, 76, 548–570.

——— (1973) Experimental studies of igneous rock series, central Sierra Nevada batholith, California: Part II. Neues Jahrbuch für Mineralogie Monatshefte, 5, 193–215.

Shannon, W.M. (1989) Middle Proterozoic alkaline granites, Franklin Mountains, El Paso, Texas (abs.). Continental Magmatism, New Mexico Bureau of Mines and Mineral Resources Bulletin, 131, 239.

Shannon, W.M., and Barnes, C.G. (1989) Middle Proterozoic alkaline anorogenic granites, Franklin Mountains, El Paso, Texas. Geological Society of America Abstracts with Programs, 21, 199.

Spear, F.S., and Kimball, K.L. (1984) RECAMP—A FORTRAN IV program for estimating $Fe^{3+}$ contents in amphiboles. Computers and Geosciences, 10, 317–325.

Thomann, W.F. (1980) Ignimbrites, trachytes, and sedimentary rocks of the Precambrian Thunderbird Group, Franklin Mountains, El Paso, Texas. Geological Society of America Bulletin, part I, 92, 94–100.

Thompson, R.N., Morrison, M.A., Hendry, G.L., and Parry, S.J. (1984) An assessment of the relative roles of crust and mantle in magma genesis: An elemental approach. Philosophical Transactions of the Royal Society of London, A310, 549–590.

Wasserburg, G.J., Wetherill, G.W., Silver, L.T., and Flawn, P.T. (1962) A study of the ages of the Precambrian of Texas. Journal of Geophysical Research, 67, 4021–4047.

Whitney, J.A. (1975) The effects of pressure, temperature, $X_{H_2O}$ on phase assemblage in four synthetic rock compositions. Journal of Geology, 83, 1–31.

Wones, D.R. (1981) Mafic silicates as indicators of intensive variables in granitic magmas. Mining Geology, 31, 191–212.

MANUSCRIPT RECEIVED MAY 23, 1990
MANUSCRIPT ACCEPTED APRIL 18, 1991